Paper 79

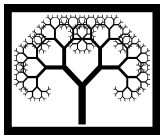

Proceedings of the Eleventh International Conference
on Computational Structures Technology,
B.H.V. Topping, (Editor),
Civil-Comp Press, Stirlingshire, Scotland

Damage Detection for Beams subject to Moving Loads based on Wavelet Transforms

J.M. Machorro-López, A. Bellino, S. Marchesiello and L. Garibaldi
Department of Mechanical and Aerospace Engineering
Politecnico di Torino, Italy

Abstract

This paper provides an efficient method based on wavelet transforms in order to detect and localize damage on structures subjected to moving loads. Two different models based on the characteristics of the test-rig utilized in this study are developed. An analytical model consisting in a concentrated mass passing over an Euler-Bernoulli beam is created, where damage is modeled as a rotational spring. On the other hand, a finite element model is also developed, different types of damage on the bridge are simulated and transient analyses are performed by incorporating a load which moves constantly along the beam nodes.

Continuous wavelet transform diagrams using the vibration responses show that damage can be identified and localized even with significant percentages of noise. Nevertheless, the method is improved by filtering the signals, removing the border effects, and calculating the total wavelet energy of the beam from the coefficients along the selected range of scales. Thus, the accumulation of wavelet energy could indicate the presence of damage. Finally, laboratory experiments are conducted to validate this work.

Keywords: damage, beams, bridges, moving loads, wavelets, finite element method, analytical model, experiments.

1 Introduction

Early damage detection on structures plays a very important role for ensuring safety and reliability. There exists a wide variety of beam-like structures which are subjected to moving loads. Some examples of these kinds of structures include bridges, fluid pipes, overhead cranes, gun barrels, rails, and work pieces on machine tools. All the load-carrying structures accumulate damage that is usually caused by degradation and deterioration of some components and/or connections during their

service life. The particular case of the bridges has been intensively studied among many others since a damage that is not early detected in this kind of civil constructions may lead to structural failure and the loss of human lives besides the huge economic losses.

Many accidents with catastrophic consequences due to collapse of bridges have occurred even in the most developed countries. One of the first most awful tragedies involving the collapse of a bridge was the called Ashtabula River Railroad Disaster, which was a train disaster caused by bridge failure in far northeastern Ohio, USA on December 29, 1876. The bridge fractured while the train was passing over and plunged 21 m into the water; 64 people were injured and 92 died. The reason of the collapse of the bridge was fatigue failure of cast iron lug pieces which were used to anchor the wrought iron bars of the truss together. This disaster helped focus efforts to draw up standards for bridges including adequate testing and inspection [1].

Only 3 years later a similar accident took place in Scotland, UK, when the Tay Rail Bridge collapsed during a violent storm while a train passed over it causing 75 people to lose their lives. The bridge failed because of structural deterioration and wind load exceeding the estimated [2]. On the other hand, on December 15, 1967, the Silver Bridge, which was an eyebar-chain suspension bridge connecting two cities over the Ohio River in USA, collapsed while it was full of rush-hour traffic, resulting in the deaths of 46 people. Investigation of the wreckage pointed to the cause of the collapse being the failure of a single eyebar in a suspension chain, due to a small defect 2.5 mm deep. The bridge had been poorly maintained and the damage was not detected early enough [3].

Likewise, recently the eight-lane steel truss arch bridge known as Bridge 9340 catastrophically failed during the evening rush hour on August 1, 2007, collapsing to the Mississippi River in Minneapolis, Minnesota, USA. Thirteen people were killed and 145 were injured. The bridge carried 140,000 vehicles daily and after the collapse the government advised to inspect the 700 bridges of similar construction in the country after a possible design flaw in the bridge was discovered, related to large steel sheets called gusset plates which were used to connect girders together in the truss structure [4].

The accidents previously described are some examples which show the need of providing an efficient method to assess the structural state of bridges and detect damage before a disaster could be caused due to the collapse of these constructions.

Some of the most used damage detection methods are based either on visual inspections or localized testing such as ultrasonic, magnetic-particle, liquid penetrant, and eddy current. However, the disadvantage of these non-destructive assessments is that they cannot be efficiently applied to big and complex structures, like the case of the bridges, because many of their parts are not easily reached for visual examination; whereas the localized testing methods can be carried out only in some elements where the possibilities of having a damage are higher or at locations where previous studies suggested that a damage could be present. Thus, damage might be accumulating in sections that were not evaluated and grow until the fracture and collapse of the structure.

Therefore, the implementation of damage detection strategies based on analyses of the vibration measurements for structural health monitoring (SHM) have been

widely used in the last three decades because they overcome the limitations of the techniques above mentioned.

Several researchers like Farrar and Jauregui [5,6] have presented comparative studies of damage identification algorithms applied to a bridge, and found that standard modal properties such as resonance frequencies and mode shapes are poor damage indicators. Consequently, this article presents a new approach to identify and localize damage based on post-processing of vibration signals using wavelet transforms (WT). The use of WT has been proposed in the recent years as a promising mathematical tool to deal with this problem. Liew and Wang [7] notified that crack identification on simply supported beams is much more efficient by using WT instead of eigenvalues analysis. They showed that the wavelet coefficients calculated along the beam presented a maximum at the crack location.

On the other hand, Surace and Ruotolo [8] developed a technique using the WT to detect a single crack in a simple cantilever beam. The vibration signals from a single accelerometer were analyzed. Likewise, Quek et al. [9] presented WT-based analyses to accurately identify small cracks in beams under both simply supported and fixed-fixed boundary conditions. Douka et al. [10] used the continuous wavelet transform (CWT) to determine the location and size of a crack in a beam using the fundamental mode of vibration. The location of the crack was found depending on the ridge of the wavelet coefficients, whereas its size was related to the magnitude of the wavelet coefficients. Similar results were also reported by Gentile and Messina [11] who showed that by means of the CWT it is possible to detect and localize damage as well as estimate its size from both noisy and clean data.

Recently, Zhu and Law [12] proposed a new method for crack identification on bridges under a moving load using wavelet analysis. The locations of the cracks were determined from the sudden changes in the spatial variation of the transform responses; moreover, they established a damage factor to calculate approximately the size of the cracks based on the coefficients of the WT diagrams.

This paper presents numerical, analytical, and experimental analyses based on WT in order to provide an efficient method to identify and localize damage on structures subjected to moving loads such as beams and bridges.

A numerical model considering the experimental test-rig utilized in this study is developed by using ANSYS®, which is a commercial software based on the finite element method (FEM). Beam elements characterize the bridge whereas the supports are modeled with spring-damper elements. Different types of damage on the bridge are simulated and transient analyses for healthy and damaged cases are performed by incorporating a load which moves along the beam nodes at constant speed. Both the displacement and the acceleration vertical responses are collected in the time domain for all the nodes and for the complete lasting of the load crossing the beam.

Likewise, a MATLAB® code is written to post-process the data obtained from the FEM simulations. CWT diagrams using the vibration responses show that if a convenient mother wavelet is selected, damage can be detected and localized even when significant percentages of white Gaussian noise are added to the original signals. Nevertheless, the damage recognition method is improved by filtering the noisy signals, removing the border effects from the CWT diagrams, and selecting an

adequate range of scales, which must be far away from the corresponding first natural frequency of the system to properly allow the identification.

In this way, the wavelet diagrams become clearer to identify and localize damage; therefore, the total wavelet energy of the beam is obtained from the coefficients along the selected range of scales for each point of the beam. Thus, following this method, a few points of measurement for the healthy and damaged numerical beams are selected and their corresponding wavelet energies are calculated. The results indicate that the total wavelet energy for an undamaged beam is very flat and there are no significant evidences of accumulation in specific parts of the beam; on the other hand, prominent peaks of wavelet energy in the neighbourhood of the damage location are observed for damaged beams. Lastly, an average of the total wavelet energy considering different points of measurement is calculated and it is shown that the percentage of error between the position of the maximum energy for damaged cases and the damage location is very small. Moreover, the intensity of damage could be estimated with the magnitude of those wavelet energy peaks.

The mathematical justification of the FEM results is carried out by developing an analytical model where a train wagon transiting over a railway bridge is modeled as a concentrated mass passing over an Euler-Bernoulli beam; whereas the damage on the beam is modeled as a rotational spring whose stiffness can be changed for simulating different magnitudes of damage.

Finally, laboratory experiments are conducted to validate this work using a test-rig composed by an aluminium bridge with flexible supports. The vertical responses are acquired with fourteen accelerometers attached along the bridge while a crossing load, which simulates a train wagon, passes over the bridge. Damage is represented by the attached masses over the bridge. The same damage detection and localization method above described for the numerical simulations is applied also for the experiments and a good agreement between experimental and numerical/analytical results is obtained.

2 Fundamentals of wavelet transform

The fast Fourier transform (FFT) is a useful tool to analyze the frequency components of a signal. However, since the FFT is the sum over all time of a signal *f(t)* multiplied by a complex exponential (see Equation (1)), the main disadvantage of using this transform is that we cannot know the instant that a particular frequency rises and, therefore, it is not a suitable tool to be used for localizing structural damage with precision.

$$F(w) = \int_{-\infty}^{\infty} f(t) e^{-jwt} dt \tag{1}$$

Likewise, the discrete Fourier transform (DFT) can provide accurate frequency information, but no time information. Thus, DFT-based SHM methods might

recognize the presence of damage by analyzing the frequency peaks while the time information would be lost. Unless a time resolution analysis is used, the value of such time information in structural vibration signals cannot be assessed.

On the other hand, good time estimation can be accomplished by applying the short time Fourier transform (STFT), which uses a sliding window to find a spectrogram that gives information about time as well as frequency. However, there is still another problem with using STFT in SHM applications: the width of window is fixed and limits the resolution in frequency. Thus, there remains a need for multiple resolution analysis that can provide fine time resolution for long duration signals and fine frequency resolution for high frequency signals [13].

The wavelet transform (WT) is a relatively new and powerful tool in the field of signal processing for SHM, which overcomes the problems that other techniques based on vibration signals measurements/analyses, like the ones based on Fourier transforms, face. This is because WT are based on a windowing technique with variable-sized regions, which is capable of using long time intervals (large window) where precise low frequency information is needed, and short time intervals (small window) where precise high frequency information is desired.

Wavelet-based methods have recently been considered as a solution in processing of non-stationary signals for structural damage detection, this is because they provide accurate location of the transient signals while reporting the fundamental frequency and its subharmonics, they do not require neither the analysis of the complete structure nor any knowledge of the material properties. Moreover, by means of the WT it is possible to perform a local analysis of a signal without losing spectral information. This property is important to reveal hidden aspects and detect damage.

The WT are based on small wavelets with limited duration known as mother wavelets, they are the basis functions in wavelet analysis and are defined by two parameters: translation and scale. The translated-version wavelets locate where we concern; whereas the scaled-version wavelets allow analyzing the signal at different scale. For a wavelet of order N, the mother wavelet can be represented as:

$$\psi(n) = \sum_{j=0}^{N-1} (-1)^j c_j (2n + j - N + 1) \tag{2}$$

where c_j represents the coefficient. Thus, the mother wavelet has to satisfy two conditions: it must integrate to zero, that is:

$$\int_{-\infty}^{\infty} \psi(t) dt = 0 \tag{3}$$

and it must be square integrable or, equivalently, it must have finite energy, that is:

$$\int_{-\infty}^{\infty} |\psi(t)|^2 \, dt < \infty \tag{4}$$

It is important to notice that Equation (3) suggests that the mother wavelet must have a wavy shape; whereas Equation (4) means that most of the energy in the mother wavelet is restricted to have a finite duration. Moreover, another property of the mother wavelets is that their values are non-zero for finite intervals.

On the other hand, the continuous wavelet transform (CWT) is defined as:

$$W(a,b) = \frac{1}{\sqrt{a}} \int f(t) \cdot \psi^* \left(\frac{t-b}{a} \right) dt \tag{5}$$

where a and b are the scale and translation parameters, respectively; whereas ψ^* is the complex conjugate of ψ. Then, the mother wavelet ψ can be represented as:

$$\psi_{j,k}(t) = 2^{j/2} \psi \left(2^j t - k \right) \tag{6}$$

If the parameter a is $0 < a << 1$, the windows will be very narrow and therefore high frequency components of the signal $f(t)$ might be analyzed; otherwise, if $a >> 1$, the windows will be very wide and low frequency components might be analyzed. According to the Heisenberg uncertainty principle, the resolution in time and frequency is given by [14]:

$$\Delta t \, \Delta f \geq \frac{1}{4\pi} \tag{7}$$

since Δf is proportional to the center frequency f, we obtain that:

$$\frac{\Delta f}{f} = C \tag{8}$$

where C is a constant. This property helps to overcome the restriction of the STFT in the sense that the time-frequency resolution is fixed. Likewise, in order to obtain an inverse wavelet transform, the mother wavelet has to satisfy the admissibility condition, which is defined as:

$$\int_{-\infty}^{\infty} \frac{|\Psi(w)|^2}{|w|} dw < \infty \tag{9}$$

where Ψ is the Fourier transform of ψ, then Equation (5) can be represented as:

$$W(a,b) = \left\langle f(t), \psi^*_{a,b}(t) \right\rangle \tag{10}$$

Thus, the CWT is a collection of inner products of a signal $f(t)$ and the translated and dilated wavelets $\psi_{a,b}(t)$. The value of the scale a is proportional to the reciprocal of the frequency, which results from:

$$F\left[\psi(t/a)\right] = |a|\,\psi\left(aw\right) \tag{11}$$

where F [ ] denotes the Fourier transform. In fact, the value of the scale a is related with a pseudo-frequency value: this latter parameter gives us an idea about the value of the corresponding vibration frequency for a specific value of scale and it can be calculated by using the following relationship:

$$F_a = \frac{F_c}{a \cdot \Delta} \tag{12}$$

where: F_a is the pseudo-frequency corresponding to the scale a, F_c is the center frequency of the mother wavelet, a is the scale, and Δ is the sampling period. In this way, a relatively low scale a implies compressed wavelets, rapidly changing details, and high vibration frequencies; whereas a relatively high scale a involves stretched wavelets, coarse features slowly changing, and low vibration frequencies.

3 Analytical model and simulations

A train wagon passing over a railway bridge can be modeled as a concentrated mass moving over a beam. Analogously to [15,16], let us consider an Euler-Bernoulli beam of length L_b, simply supported at the ends, travelled by a mass m with constant speed v (see Figure 1). In order to simulate a damage on the beam, a crack is placed at $x=L_c$, with relative depth $p=\delta/h_b$, where δ is the depth of the crack.

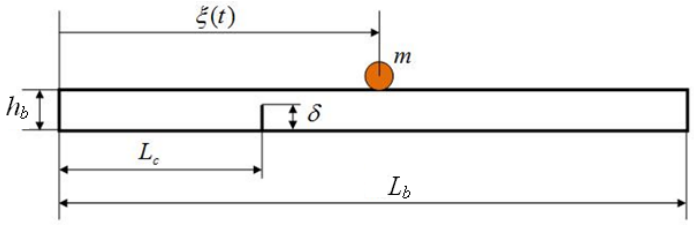

Figure 1: Damaged beam subjected to a moving mass.

The equation of motion is:

$$\rho A \frac{\partial^2 w}{\partial t^2}(x,t) + EI \frac{\partial^4 w}{\partial x^4}(x,t) = -m\left(a_v + g\right)X(t)\delta\left(x - \xi(t)\right) \tag{13}$$

where $w(x,t)$ is the vertical deflection of the beam; ρ, E, A, and I are the mass density, the Young's modulus of the material, the cross-sectional area, and the area moment of inertia, respectively; and a_v is the vertical acceleration of the moving mass. Moreover, $\xi(t)=vt$ is the instantaneous position of the mass along the beam and $X(t) = u(t) - u(t - l/v)$ is a window function, defined by unit step functions u.

By neglecting the possibility that the mass may separate from the beam and considering the mode superposition, the equation of motion of the coupled beam-mass system is obtained in the following compact form (see [15,16] for details):

$$[M(t)]\{\ddot{q}(t)\}+[C(t)]\{\dot{q}(t)\}+[K(t)]\{q(t)\}=g\{\tau(t)\} \tag{14}$$

The matrices $[M(t)]$, $[C(t)]$, and $[K(t)]$ are depending on the load mass, the load velocity, and the load position; therefore they are time-varying matrices. The vector $\{q(t)\}$ represents the modal coordinates. The crack is modeled as a rotational spring with stiffness K_t, linked to p by the following relationship:

$$K_t = \frac{EI}{6h_b\pi p^2 f(p)} \tag{15}$$

where: $f(p)=0.638-1.035p+3.720p^2-5.173p^3+7.553p^4-7.332p^5+2.491p^6$.

The time histories responses for both healthy and damaged cases were generated by integrating Equation (13) and adding 3% of white Gaussian noise. Moreover, for these simulations, the sampling frequency was selected as 300 Hz, the speed of the mass v = 0.2 m/s, and the mass of the moving load was m = 2.5 kg; the dimensions and material properties of the beam corresponded with those of the experimental aluminium bridge shown later in Section 5 (L_b=1.86 m, b_b=0.15 m, h_b=0.015 m, E=70 GPa, and ρ=2700 kg/m^3). The damaged case consisted in a crack located at 0.66 m from the left side and with p=0.8, which does not mean a huge damage since the crack is punctual. In other words, also the part of the beam closest to the crack concurs to confer flexural rigidity to the beam. This is a limit of the crack model adopted. By considering our crack configuration, the diminution of the first natural frequency was equal to 6.34%.

In Figure 2, the displacement responses for the healthy and damaged cases are presented as well as their corresponding CWT diagrams by using the Mexican hat mother wavelet. Thus, it is possible to see a significant indicator of damage in the respective CWT diagram, which is highlighted by attaching a black circle. These first results will be validated later with FEM and experimental analyses and constitute the initial motivation to develop a formal method based on wavelets for detecting and localizing damage, which is presented in the next section.

All the mother wavelets were analyzed for this first set of simulations and it was found that the most promising mother wavelet to detect damage was the one called Mexican hat. Thus, all the WT analyses performed in this paper were based on using this mother wavelet. The Mexican hat mother wavelet is a function which is proportional to the second derivative function of the Gaussian probability density function, its center frequency is equal to 0.25 Hz, and it is represented as follows:

$$\psi(t)=\left(\frac{2}{\sqrt{3}}\pi^{-1/4}\right)\left(1-t^2\right)e^{-t^2/2} \tag{16}$$

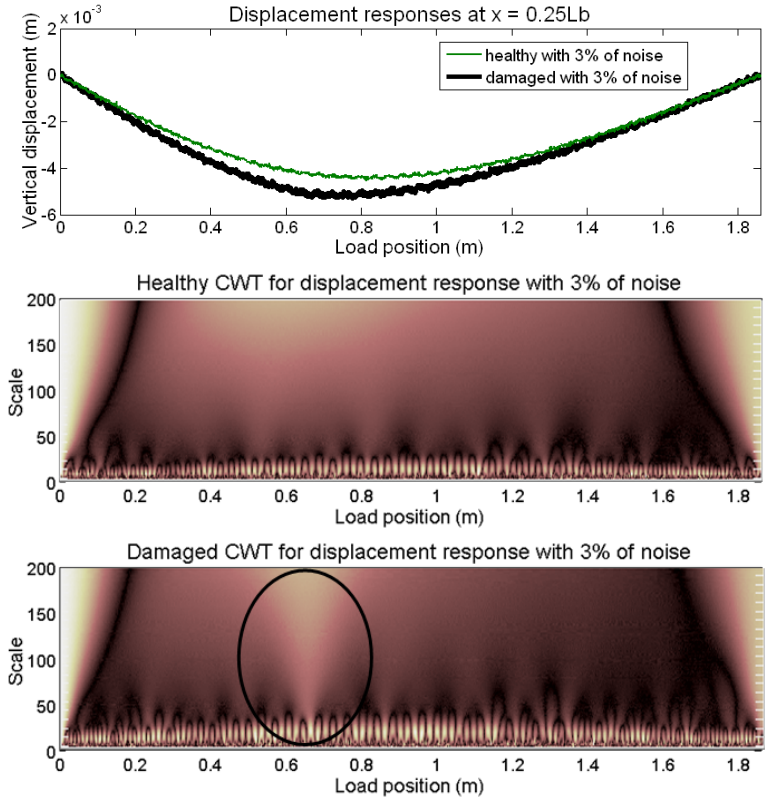

Figure 2: Analytical displacement responses measured at $0.25L_b$ and corresponding CWT diagrams for healthy and damaged (L_c = 0.66 m) cases with 3% of noise.

4 FEM-based model and simulations

Another simple but versatile model was created with the FEM-based commercial software ANSYS® version 12.1 to represent the experimental test-rig used at the laboratory for this study. The 1.86 m length bridge was simulated by using 2-D elastic beam elements type BEAM3, which are uniaxial elements with tension, compression, and bending capabilities. They have three degrees of freedom (DOF) at each node: translations in the x and y directions and rotation about the z-axis.

The supports of the bridge were represented by incorporating longitudinal COMBIN14 spring-damper elements at the ends of the total beam in the three Cartesian directions: vertical, horizontal, and axial. COMBIN14 is a uniaxial tension-compression element and, for simplicity purposes, the damping was neglected and the value of the stiffness for the springs in the three directions was adjusted according with the experimental configuration of the test-rig and its equivalent values of natural frequencies. Both elements used are shown in Figure 3.

Furthermore, damage on the bridge can be simulated with this model in different ways: by changing the cross-sectional geometric characteristics of a specific part of the beam, by changing the material properties (Young's Modulus) of a specific part of the beam, by attaching a mass element type MASS21 on a specific node of the

beam, or combinations thereof. However, for our simulations, damage was considered just by changing the cross-sectional geometric characteristics of one element equivalent to 5% of the beam length. On the other hand, the wagon which passes over the experimental bridge was characterized as a constant load that moves at constant speed along the nodes of the beam. For this model, the inertial effects were neglected.

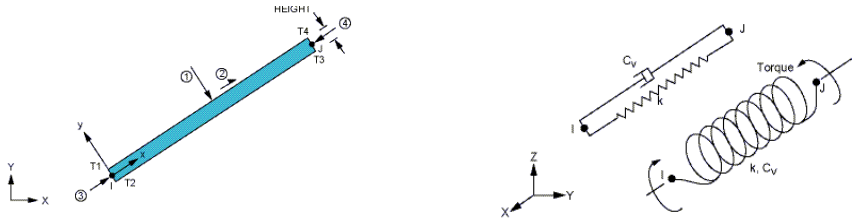

Figure 3: FEM elements used for representing the bridge (BEAM3) and the supports (COMBIN14), respectively.

An efficient code was written in ANSYS® which allows easily changing the parameters of the model and performing different solutions such as static, modal, and transient. The complete FEM model can be seen in Figure 4, which contains 28 elements (20 for the beam and 8 for the supports) for a total of 29 nodes.

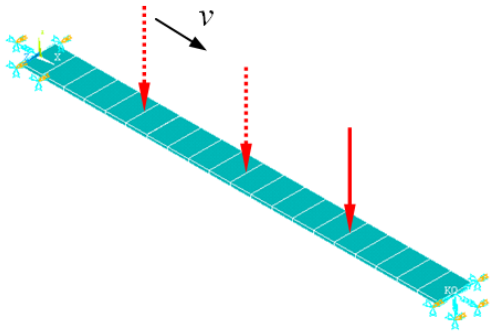

Figure 4: Final FEM model with constant load moving along the beam nodes.

Since the objective of this work is to detect damage on the bridge by using WT, both the displacement and the acceleration vertical responses were collected in the time domain for all the beam nodes and for the complete lasting of the load crossing the beam. Therefore, transient analysis had to be performed and it was found that the quantity of elements selected was the most convenient in function of the parameters of the simulations (speed of the moving load and sampling frequency), computing time, and precision of results.

The first set of FEM simulations consisted in comparing a healthy bridge against a damaged bridge with a crack of 50% of the beam height (p = 0.5) located at 0.66 m from the left end (D1). The transient simulations were performed by establishing the weight of the moving load P = 24.1 N and a sampling frequency of 300 Hz, whereas two constant speeds of the load were analyzed: v = 0.2 m/s and 0.5 m/s. All the

scenarios simulated in this section are shown in Table 1. Then, a MATLAB® code was written to post-process the signals obtained from the FEM simulations.

Case	Nomenclature	Description
1	H	Healthy beam, v = 0.2 m/s, P = 24.1 N
2	D1	Cracked beam (p = 0.5 at 0.66 m), v = 0.2 m/s, P = 24.1 N
3	D2	Cracked beam (p = 0.4 at 0.66 m), v = 0.2 m/s, P = 24.1 N
4	D3	Cracked beam (p = 0.3 at 0.66 m), v = 0.2 m/s, P = 24.1 N
5	D4	Cracked beam (p = 0.2 at 0.66 m), v = 0.2 m/s, P = 24.1 N
6	D5	Cracked beam (p = 0.1 at 0.66 m), v = 0.2 m/s, P = 24.1 N
7	D6	Cracked beam (p = 0.4 at 1.40 m), v = 0.5 m/s, P = 24.1 N

Table 1: Scenarios numerically simulated with ANSYS®.

Once again, all the mother wavelets were analyzed for this first set of FEM simulations and, as it was notified in the previous section of this paper, the most promising mother wavelet for detecting damage was the Mexican hat.

In Figure 5 the time history vertical displacement responses measured at the mid-span and the corresponding CWT diagrams are shown for the healthy case without noise as well as with 15% of white Gaussian noise, and it can be observed that there are no evidences of damage.

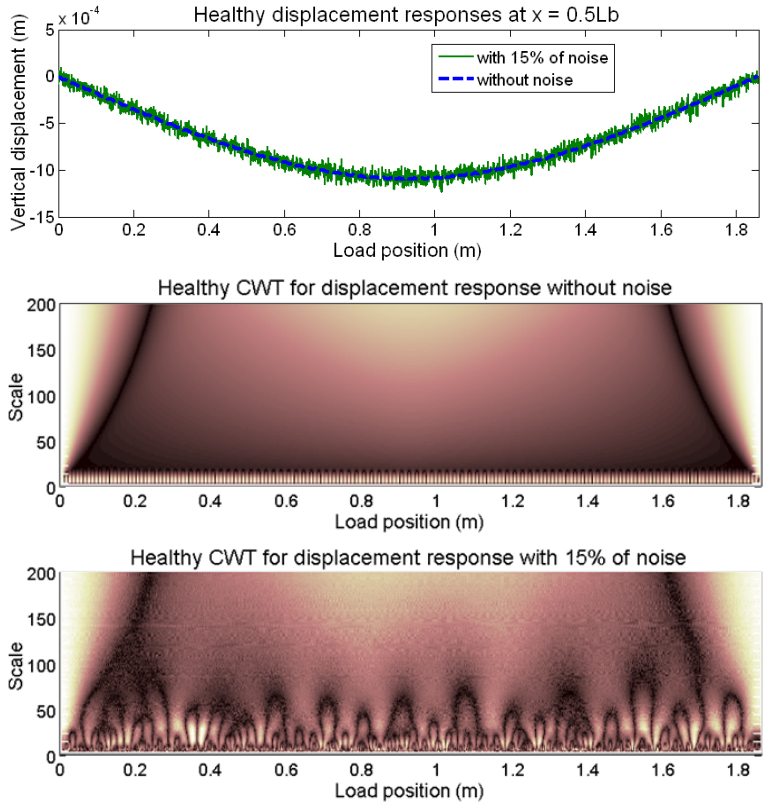

Figure 5: Mid-span displacement responses and CWT diagrams for healthy case.

On the other hand, if damage is included on the beam at 0.66 m from the left side (see Figure 6); it is clear that the CWT diagrams present an indicator of the damage presence practically at the exact location of the damage even when 15% of white Gaussian noise was added to the original signal. The dark tonality in the CWT diagrams indicates low magnitude coefficients, whereas bright tonalities indicate high magnitudes for the coefficients. In this way it is possible to notice that there is a significant change of tonality in the damaged CWT diagrams around the location of the crack, which becomes very bright. These results match very well with corresponding analytical simulations previously presented in Section 3.

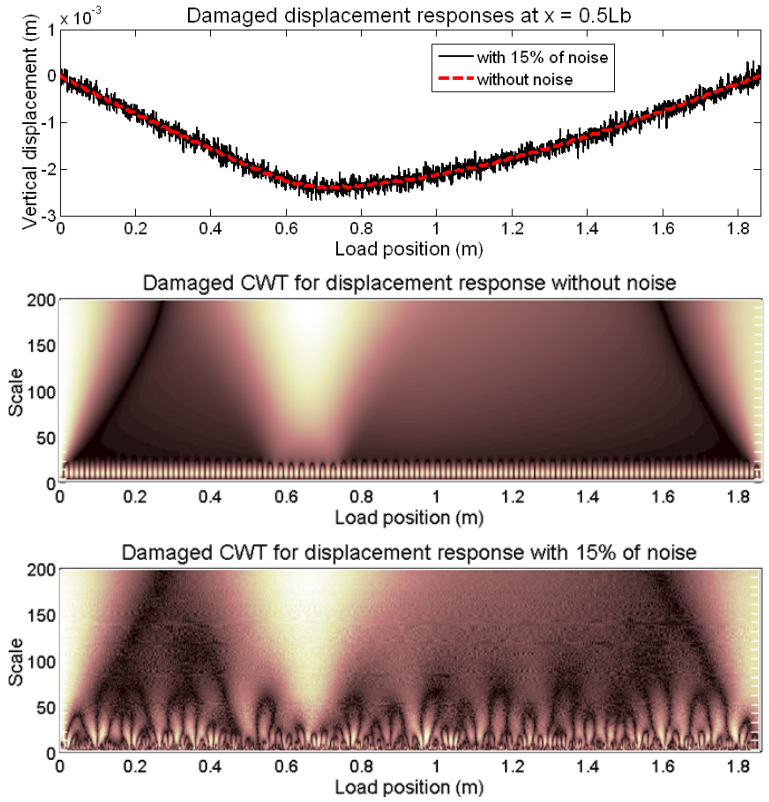

Figure 6: Mid-span displacement responses and CWT diagrams for damaged case (D1).

The latter results are very promising for detecting and localizing damage, but since for practical cases the acceleration responses are measured instead of the displacement responses, the same simulations above presented were performed again but collecting the accelerations responses. In this case, the damage was also easily detected and localized for original signals and noisy signals with a maximum of 7% of white Gaussian noise, which is still very high, considering that in most of the methods for detecting structural damage, the added noise is not higher than 3%. The responses were measured again at the beam mid-span and the evidence of damage was clear. The acceleration responses and the CWT diagrams for the healthy case are presented in Figure 7, whereas the corresponding diagrams for the damaged case (D1) are shown in Figure 8.

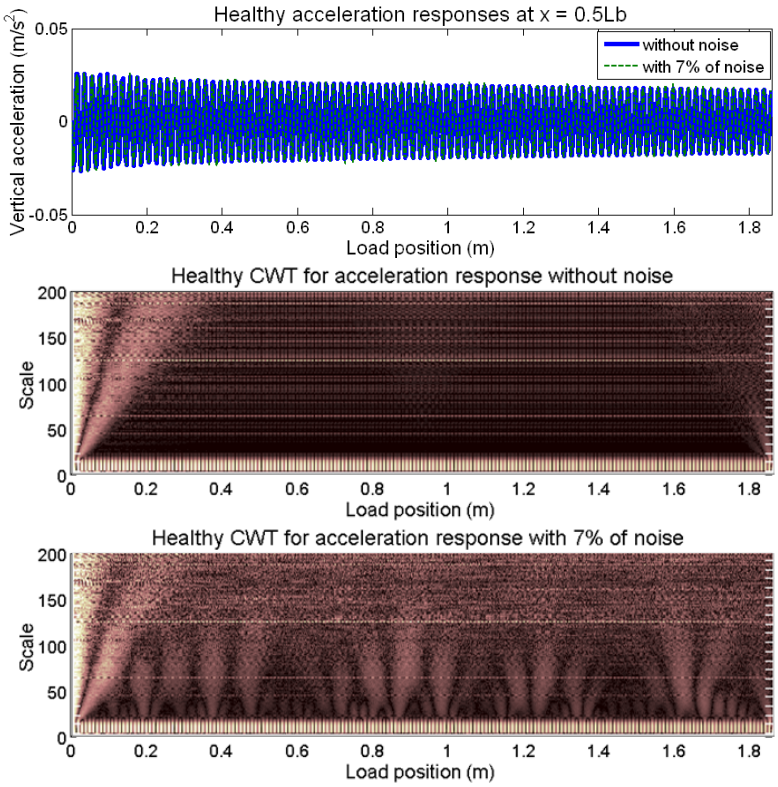

Figure 7: Mid-span acceleration responses and CWT diagrams for healthy case.

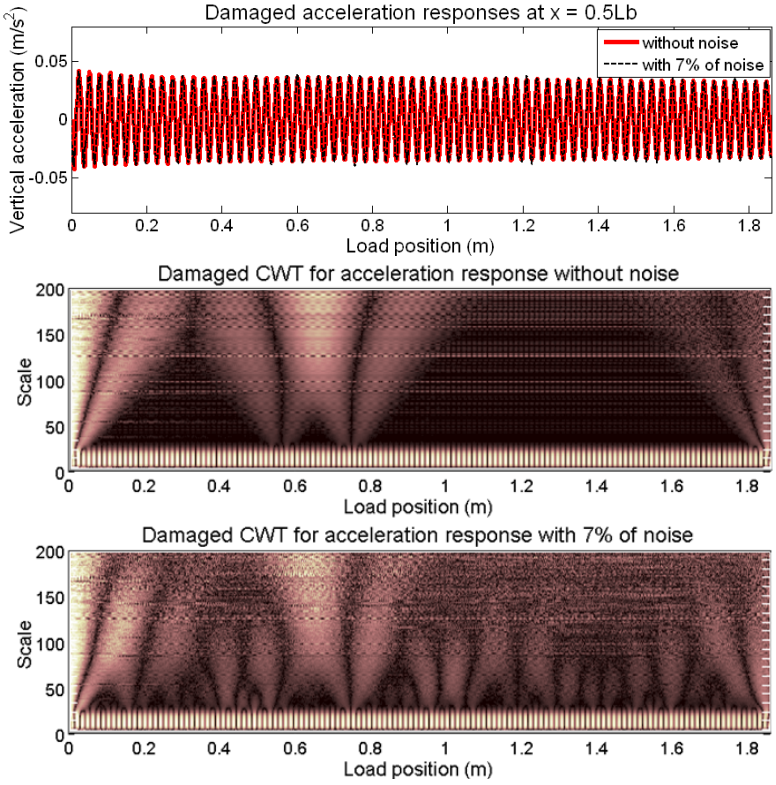

Figure 8: Mid-span acceleration responses and CWT diagrams for damaged case (D1).

After analyzing the CWT diagrams presented in Figure 8, the possibilities of detecting and localizing damage with this technique are very heartening, but there are still several aspects that can be improved in order to obtain a more precise and formal method. Those aspects to be improved and the corresponding solutions are described in the next steps, which constitute the method suggested in this article for detecting and localizing damage:

1) For a real case, the acceleration signals will always contain noise but some noise can be advantageously removed; then, in order to increase the evidence of damage, a Savitzky-Golay filter, which is a smoothing polynomial filter, is designed and the filtered signals are analyzed instead of the noisy ones.

2) A feature contained in the CWT information must be selected as the first parameter for the identification and localization of damage, then the coefficient is selected as our first damage indicator.

3) The border effects of the CWT diagrams can obstruct the damage detection because they contain high magnitude coefficients which can be considered as damage; therefore, this effect is removed by eliminating a small percentage of the first and last part of the filtered signals, then those trimmed signals are padded with the corresponding first and last five cycles, and lastly the padded signals are extended (i.e. the added parts are repeated several times) to bring the border effects to "inexistent" parts of the beam (before and after the real ends of the beam): in this way the border effects will not be present in our analysis.

4) A convenient range of scales must be selected to analyze the coefficients into a limited area of the CWT diagrams without the influence of the first natural frequency and the higher ones. As it can be observed in Figures 5 - 8, the effect of the first natural frequency (which is 10.01 Hz for the healthy case and 7.24 Hz for the damaged case, corresponding approximately to a scale of 7.49 and 10.36, respectively), is very evident; therefore, a range of scales far away from the first natural frequency is chosen from 100 to 200.

5) With the previous steps, the CWT diagrams become clearer to identify and localize damage; now a second damage parameter must be considered as the principal feature to detect and localize damage: the total wavelet energy of the bridge, which is based on the first damage indicator. This latter parameter is obtained by calculating the area under the curve formed by the coefficients along the selected range of scales for each point of the beam. Lastly, an average of the total wavelet energy considering different points of measurement is obtained and the accumulation of this energy in specific parts of the beam will suggest the presence and location of damage.

The MATLAB® code written to post-process the data makes this process above described automatically and Figure 9 shows the filtered signal obtained from the noisy damaged acceleration signal presented in Figure 8 after being trimmed, padded, and extended as described in the step 3).

Therefore, the yellow square attached in the CWT diagram of Figure 9 indicates the convenient area to calculate the total wavelet energy and detect damage; it can be observed that into this square there are neither the effects of the first natural frequency nor the border effects anymore; and even more, since the noisy signal was filtered, the diagram is clearer and the presence of damage is more evident.

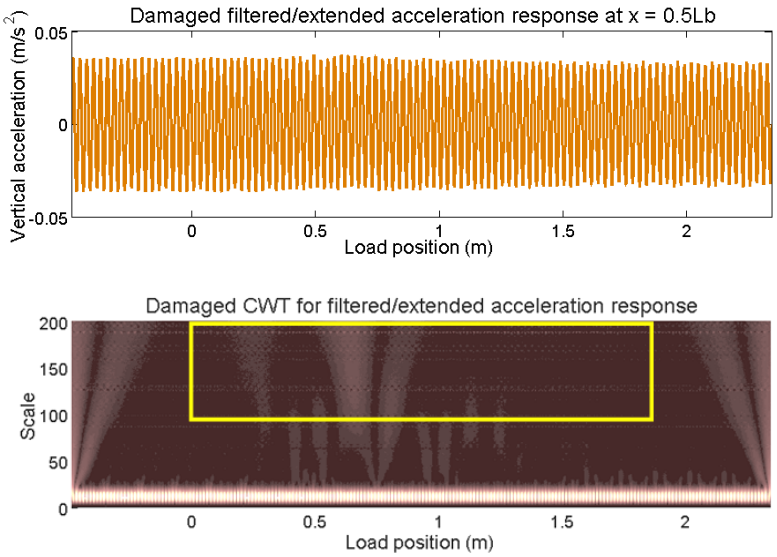

Figure 9: Mid-span filtered acceleration signal after being trimmed, padded, and extended; and corresponding CWT diagram for damaged case (D1).

Thus, in Figure 10 it is exhibited the total wavelet energy of both healthy and damaged beams considering 3 points of measurement at $0.25L_b$, $0.5L_b$, and $0.75L_b$ (where L_b, is the total length of the beam), as well as the corresponding average of the wavelet energy for those points of measurement. The wavelet energies for the healthy case are very flat and there are no parts of the beam with significant accumulation of energy; in fact, the maximum level of the average wavelet energy (occurring at 1.14 m) is very close to the minimum level of average wavelet energy, and therefore there is no any significant peak of energy which could suggest the presence of damage.

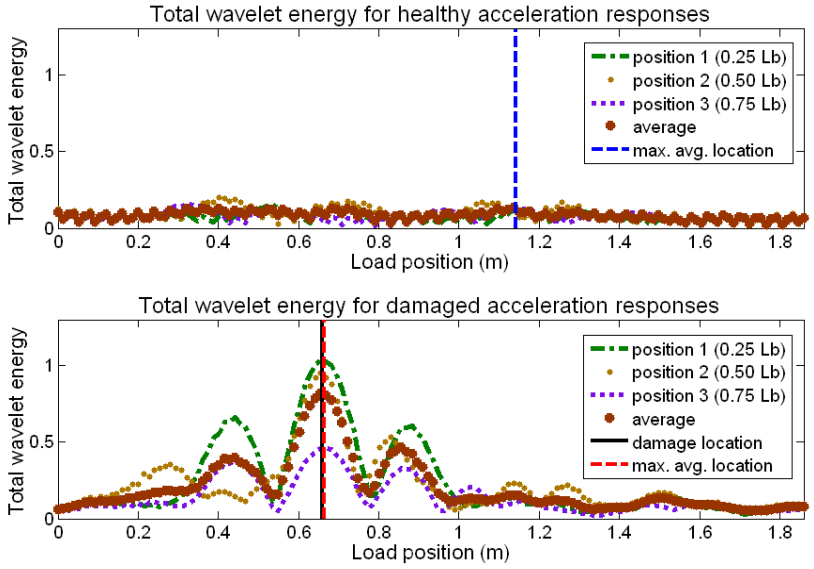

Figure 10: Total wavelet energy for healthy case and damaged case (D1).

On the other hand, for the damaged case, it is evident that for all the points of measurement there exists a significant peak of energy in the neighbourhood of the damage; and as a consequence, the maximum level of the average energy occurs at 0.6643 m, therefore, the percentage of error between the position of the maximum peak of the average energy for this damaged case and the location of the damage is 0.65%, which is very small; the vertical solid line represents the position of the damage, whereas the vertical dashed lines indicate the position of the maximum energy for the average. In this way, following this method, the recognition of damage is possible and its localization is very precise.

Finally, the average wavelet energies for all the cases presented in Table 1 are shown in Figure 11, where it is possible to see that the maximum peak of energy for all the damaged cases occurs in the vicinity of the corresponding damages locations. The case with the smallest damage (D5) does not present a significant prominent peak of energy but at least its maximum level of energy occurs around the damage location; in fact, following this method, the percentage of error in the localization of damage for the cases D1-D5 was less than 1.40%, whereas the corresponding percentage of error for the case D6 increased until 3.86% due to the increment of speed and the needing of a better resolution (sampling frequency), but still that percentage of error is very acceptable. Furthermore, the damaged cases D1-D5 have the same conditions and only the intensity of damage was modified; thus, if their energy curves are observed, it is evident that the magnitude of the maximum peak of energy increases if the damage also increases. Therefore, the method here proposed could detect, localize, and classify damage according with its intensity on structures subjected to moving loads.

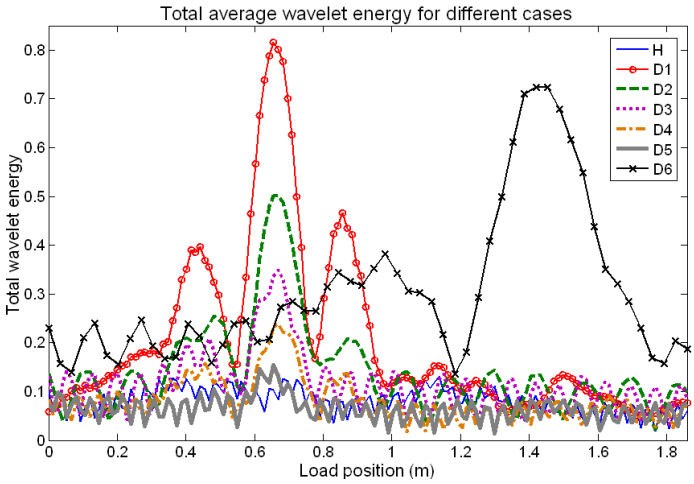

Figure 11: Total average wavelet energy for all the cases presented in Table 1.

5 Experimental validation

The experimentation conducted to validate this research was carried out at the Laboratory of the Department of Mechanical and Aerospace Engineering of

Politecnico di Torino. The test-rig utilized consisted in two rigid bridges connected by an elastic aluminium bridge whose supports try to simulate a simply supported beam. A plastic/aluminium ballast was placed on the bridges and the vertical acceleration responses were acquired and collected by using an OROS-38® acquisition system and fourteen accelerometers attached along the elastic bridge while a plastic car, which represents a train wagon, passed over the ballast-elastic bridge. The mass of the car was 0.46 kg and a mass of 2 kg was added on the car for a total moving mass of 2.46 kg. The dimensions of the elastic bridge, which was the element under study, were: total length L_b = 1.86 m, base b_b = 0.15 m, height h_b = 0.015 m. Since the elastic bridge could not be cracked, damage was represented by attaching a mass of 0.42 kg on the elastic bridge at 0.66 m from the left end. The mass simulating damage was equivalent to 3.37% of the ballast-elastic bridge mass and 2.81% of the mass of the group ballast-elastic bridge-total moving mass.

In Figure 12, a picture of the test-rig showing the left-side rigid bridge and the wagon before crossing the elastic bridge is included; whereas in Figure 13 it is possible to see the pictures of the whole elastic bridge instrumented and a detail of the supports for one of the ends of the aluminium bridge, respectively.

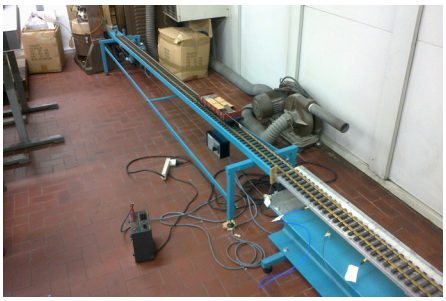

Figure 12: Picture of the test-rig showing the car before entering to the elastic bridge.

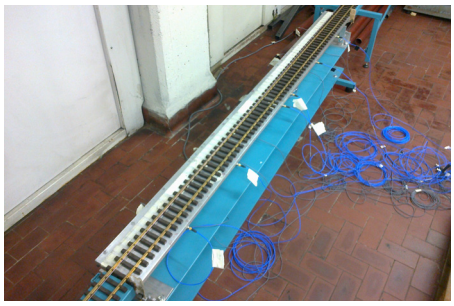

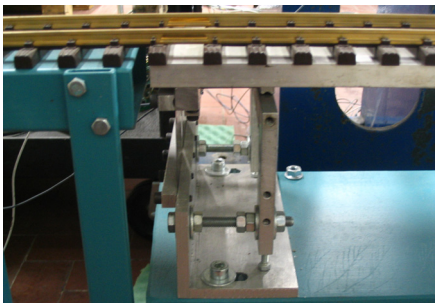

Figure 13: Pictures of the test-rig showing the instrumented elastic bridge and the detail of the supports for one end of the elastic bridge, respectively.

The car was propelled by a motor and a string. The motor was controlled by a DC power supply; therefore, the speed of the car was in function of the selected voltage. For the experiment designed to validate this work, a voltage of 5 V was selected to result in an almost constant car speed of 0.36 m/s; moreover, the experimental sampling frequency was 512 Hz.

The original damaged acceleration signal measured at $0.125L_b$, the corresponding filtered acceleration signal (selecting a polynomial order of 8 and a frame size equals to 19 as the most convenient filter parameters), as well as the respective CWT diagrams for those responses are presented in Figure 14. If the original signal is considered, the detection of damage is impossible by analyzing the CWT diagram, this is because the signal is very noisy and damage is masked; on the other hand if the signal is filtered, a significant evidence of damage appears in the CWT diagram practically at the exact position where damage was incorporated. These latter results agree very well with the previous numerical results.

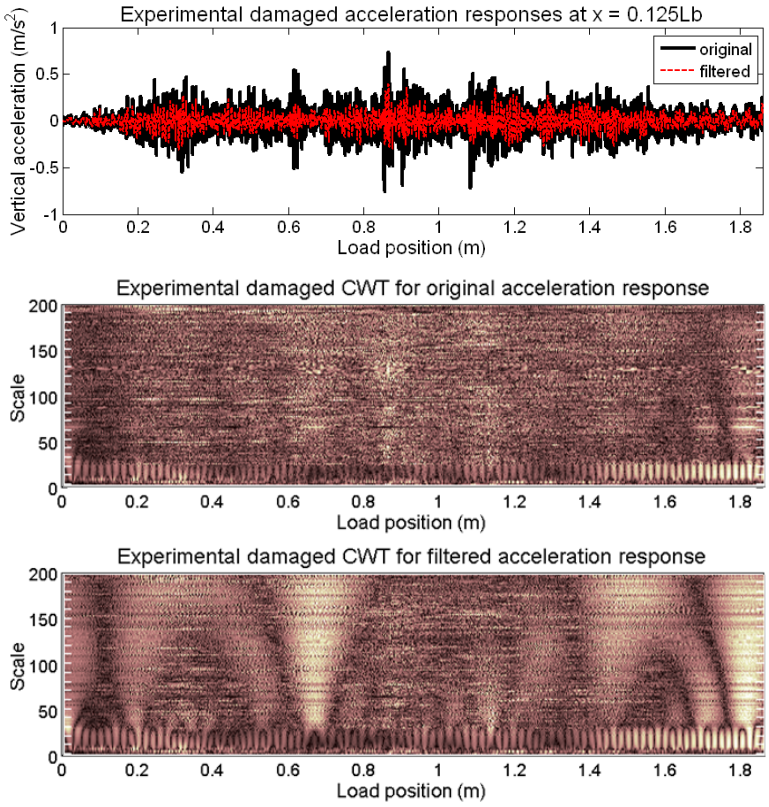

Figure 14: Experimental responses and CWT diagrams for damaged case.

Finally, the same damage detection and localization method described in the numerical part of this article is applied for the experimental results. Thus, the total wavelet energy of the damaged test-rig configuration is calculated for three measuring points of the elastic bridge ($0.125L_b$, $0.550L_b$, and $0.875L_b$); moreover, the total average wavelet energy is also estimated. The corresponding curves for those wavelet energies are presented in Figure 15 and it can be notified that the maximum peak of energy for each measured point occurs in the neighbourhood of the damage location except for the third position, where the energy peak related with the damage is the second one in magnitude.

However, if an averaging of the wavelet energies for the different positions is performed, the discrepancies among them can be compensated and, at the end, more

trustful information is obtained. Therefore, if the total average wavelet energy is analyzed, it is possible to see that there is one prominent peak of energy accumulation whose position is very near to the damage position. As in the Figure 10, the vertical solid line indicates the damage position and the vertical dashed line corresponds with the position of the maximum level of wavelet energy for the average case; consequently, the damage was detected and localized with an error of 3.89%. In this way, the numerical results were validated experimentally with a good agreement between them.

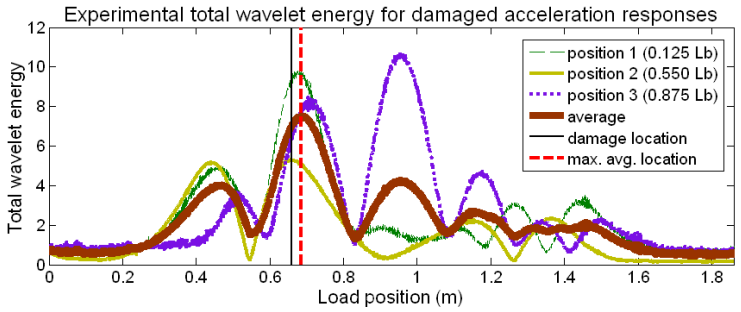

Figure 15: Experimental total wavelet energy for damaged case.

6 Conclusion

In this paper we presented an efficient method based on continuous wavelet transform (CWT) diagrams to detect and localize damage on beam-like structures subjected to moving loads, such as bridges. The method is suitable for displacement responses as well as for acceleration responses and consists of calculating, for many different points along the beam, the wavelet energy from the coefficients along the selected range of scales; thus, a significant peak of wavelet energy accumulation will indicate the presence of a malfunction, whereas its location and intensity could also be estimated according with the position and magnitude of the maximum peak of wavelet energy, respectively.

Likewise, the reliability and precision in detecting and localising damage will increase if the average of a few wavelet energies corresponding to different measuring points is considered. Lastly, it is important that before calculating the total wavelet energy, the considered signals must be adequately filtered for increasing the damage evidence; and moreover, must be post-processed in such a way that the border effects of the CWT diagrams have to be removed. A good agreement among analytical, numerical, and experimental results was obtained.

Acknowledgments

The first author thanks to Consejo Nacional de Ciencia y Tecnología *CONACYT*-Mexico for the post-doctoral scholarship granted to collaborate with this research.

References

[1] T.E. Corts, “Bliss and tragedy: the Ashtabula railway-bridge accident of 1876 and the loss of P.P. Bliss”, Sherman Oak Books, Birmingham, Alabama, USA, 145-158, 2003.

[2] “Tay bridge disaster: appendix to the report of the court of inquiry”, Houses of Parliament, London, United Kingdom, 1-49, 1880.

[3] C. LeRose, “The collapse of the silver bridge”, West Virginia Historical Society Quarterly, 15(4), 1, 2001.

[4] M. Davey, M.L. Wald, “Potential flaw is found in design of fallen bridge”, The New York Times, August 8, 2007.

[5] C.R. Farrar, D.A. Jauregui, “Comparative study of damage identification algorithms applied to a bridge: I. Experiment”, Smart Materials and Structures, 7(5), 704-719, 1998.

[6] C.R. Farrar, D.A. Jauregui, “Comparative study of damage identification algorithms applied to a bridge: II. Numerical study”, Smart Materials and Structures, 7(5), 720-731, 1998.

[7] K.M. Liew, Q. Wang, “Application of wavelet theory for crack identification in structures”, Journal of Engineering Mechanics, 124(2), 152-157, 1998.

[8] C. Surace, R. Ruotolo, “Crack detection of a beam using the wavelet transform”, in Proceedings of the 12th International Modal Analysis Conference, Honolulu, Hawaii, USA, 1141-1147, 1994.

[9] S. Quek, Q. Wang, L. Zhang, K. Ang, “Sensitivity analysis of crack detection in beams by wavelet technique”, International Journal of Mechanical Sciences, 43(12), 2899-2910, 2001.

[10] E. Douka, S. Loutridis, A. Trochidis, “Crack identification in beams using wavelet analysis”, International Journal of Solids and Structures, 40(13-14), 3557-3569, 2003.

[11] A. Gentile, A. Messina, “On the continuous wavelet transforms applied to discrete vibrational data for detecting open cracks in damaged beams”, International Journal of Solids and Structures, 40(2), 295-315, 2003.

[12] X.Q. Zhu, S.S. Law, “Wavelet-based crack identification of bridge beam from operational deflection time history”, International Journal of Solids and Structures, 43(7-8), 2299-2317, 2006.

[13] C-L, Liu, “A Tutorial of the Wavelet Transform”, 1-2, February 23, 2010.

[14] H. Kim, H. Melhem, “Damage detection of structures by wavelet analysis”, Engineering Structures, 26(3), 347-362, 2004.

[15] A. Bellino, L. Garibaldi, S. Marchesiello, “Time-varying output-only identification of a cracked beam”, Key Engineering Materials, 413-414(1), 643-650, 2009.

[16] A. Bellino, A. Fasana, L. Garibaldi, S. Marchesiello, “PCA-based detection of damage in time-varying systems”, Mechanical System and Signal Processing, 24(7), 2250-2260, 2010.